Radiolysis Process Modeling Results for Scenarios

Used Fuel Disposition

Prepared for
U.S. Department of Energy
Separations/Waste Form Campaign

E. C. Buck, R. S. Wittman,
F. N. Skomurski, K. J. Cantrell,
B. K. McNamara, C. Z. Soderquist
Pacific Northwest National Laboratory

July, 2012

FCRD-UFD-2012-000199
PNNL-21554

DISCLAIMER

This information was prepared as an account of work sponsored by an agency of the U.S. Government. Neither the U.S. Government nor any agency thereof, nor any of their employees, makes any warranty, expressed or implied, or assumes any legal liability or responsibility for the accuracy, completeness, or usefulness, of any information, apparatus, product, or process disclosed, or represents that its use would not infringe privately owned rights. References herein to any specific commercial product, process, or service by trade name, trade mark, manufacturer, or otherwise, does not necessarily constitute or imply its endorsement, recommendation, or favoring by the U.S. Government or any agency thereof. The views and opinions of authors expressed herein do not necessarily state or reflect those of the U.S. Government or any agency thereof.

SUMMARY

This report satisfies the Used Fuel Disposition M3 Milestone, Radiolysis Products Modeling Results for Scenarios, (M3FT-12PN080651).

Assessing the performance of Spent (or Used) Nuclear Fuel (UNF) in geological repository requires quantification of time-dependent phenomena that may influence its behavior on a time-scale up to millions of years. A high-level waste repository environment will be a dynamic redox system because of the time-dependent generation of radiolytic oxidants and reductants and the corrosion of Fe-bearing canister materials. One major difference between used fuel and natural analogues, including unirradiated UO_2, is the intense radiolytic field. The radiation emitted by used fuel can produce radiolysis products in the presence of water vapor or a thin-film of water (including hydroxide (OH•) and hydrogen (H•) radicals, oxygen ion (O_2^-), aqueous electron (e_{aq}), hydrogen peroxide (H_2O_2), hydrogen gas (H_2), and the secondary radiolysis product, oxygen (O_2)) that may increase the waste form degradation rate and change radionuclide behavior.

Hydrogen peroxide (H_2O_2) is the dominant oxidant for spent nuclear fuel in an O_2-depleted water environment. The most sensitive parameters have been identified with respect to predictions of a radiolysis model under typical conditions. As compared with the full model with about 100 reactions, it was found that only 30 to 40 of the reactions are required to determine $[H_2O_2]$ to one part in 10^{-5} and to preserve most of the predictions for major species. This allows a systematic approach for model simplification and offers guidance in designing experiments for validation.

CONTENTS

1. Model Description 1
   1.1 Modeling Concepts and Processes 2

2. Verification, Validation, and Sensitivity Analyses 10

3. Uncertainty and Conditional Applicability 13
   3.1 Hydrogen 15
   3.2 The Role of Bicarbonate and Oxalate Formation 16
   3.3 Secondary Uranium phases 16
   3.4 Brine 17

4. Conclusions and Recommendations 18

References 20

FIGURES

Figure 1.1 The dose to the surface of used fuel exposed to a mixed water-air environment (10% water) is dominated by long-lived alpha radiation even at relatively short times out of reactor [Adapted from Radulescu 2011] 2

Figure 1.2 Schematic of reaction pathways in the radiolysis model (adapted from Sunder 1998) 3

Figure 1.3 Calculated surface environment within 30 mm of a 160 rad/s alpha field in an anoxic environment illustrating the time dependence of dominant species 4

Figure 1.4 Radiolysis Model showing generation and diffusion across spatial regions 7

Figure 2.1 Concentration history results for the same conditions (1 hr, 25 rad/s irradiation) as Pastina and LaVerne (2001, Figure 1). 11

Figure 2.2 Radiolysis model result with inputs from Christensen and Sunder (2000) 11

Figure 2.3 Radiolysis model result for gamma irradiation with inputs from Ershov and Gordeev (2008) 12

Figure 3.1 *G*-value sensitivity as $\Delta[A]/[A]$ for H_2O_2, H_2O_2 & •OH 13

Figure 3.2 Rate constant sensitivity as absolute value of $\Delta[H_2O_2]/[H_2O_2]$ 14

Figure 3.3 H_2O_2 concentration as a function of dose for fixed O_2 concentration and range of H_2 concentrations 14

Figure 3.4 H_2O_2 concentration as a function of dose rate for cases of *zero* initial O_2 concentration 15

ACRONYMS

ANL	Argonne National Laboratory
EBS	Engineered barrier system
FCR&D	Fuel Cycle Research & Development
HLW	High level waste
PNNL	Pacific Northwest National Laboratory
UFD	Used fuel disposition
UNF	Used nuclear fuel

1. Model Description

Assessing the performance of Spent (or Used) Nuclear Fuel (UNF) in geological repository requires quantification of time-dependent phenomena that may influence its behavior on a time-scale up to millions of years. A high-level waste repository environment will be a dynamic redox system because of the time-dependent generation of radiolytic oxidants and reductants and the corrosion of Fe-bearing canister materials (Stroes-Gascoyne et al. 2005, Shoesmith et al. 2003). One major difference between used fuel and natural analogues, including unirradiated UO_2, is the intense radiolytic field. The radiation emitted by used fuel can produce radiolysis products in the presence of water vapor or a thin-film of water (including hydroxide (OH•) and hydrogen (H•) radicals, oxygen ion (O_2^-), aqueous electron (e_{aq}), hydrogen peroxide (H_2O_2), hydrogen gas (H_2), and the secondary radiolysis product, oxygen (O_2)) that may increase the waste form degradation rate and change radionuclide behavior. As H_2 escapes from the water layer surface, the local conditions at the fuel/water interface (i.e., within the first 300 µm) may always be oxidizing in the α-radiolytic field even in reducing environments. Experiments with UNF are thought to be significantly influenced by their high β,γ-radiation field, which results in generation of powerful oxidizing radiolytic species (e.g., OH• and H_2O_2). However, at the fuel/water interface, the β,γ-radiation field is not as intense as the alpha field (Radulescu, 2011) (see Figure 1.1). Hence, although Shoesmith et al. (2003) has argued that it is highly conservative to use rates of reaction from relatively fresh used fuel for performance assessment calculations; surface radiolytic calculations indicate that the β,γ-radiation field is not impacting the surface reactions. Burns et al. (2012) have argued that the oxidizing nature of a repository should be one of the most important selection criterions for the long-term disposal of used fuel. Higher oxidation rates would indeed be predicted by the corrosion models in the presence of atmospheric concentrations of O_2; however, the radiolytic field from the fuel surface will result in localized oxidizing conditions. Reducing geologic environments have been suggested by Burns et al. (2012) for UNF that are similar to those planned for the Swedish nuclear waste disposal program. The Swedish repository design also incorporates large quantities of cast iron, embedded in bentonite at a depth of about 500 m in granitic bedrock. An H_2 pressure of 50 bar (725 psi) has been predicted to be generated from the anoxic corrosion of the iron canisters by groundwater (Cui et al. 2012). Dissolved hydrogen at low temperature is chemically inert and can significantly contribute to establishing reducing conditions in the near field (Carbol et al. 2009, Ekeroth et al. 2006, Jégou et al. 2005) and effectively shutting down the UO_2 oxidation process.

However, for the case of the localized corrosion of used fuel, because the alpha field is dominant, some fuel corrosion should occur under any conditions if water contacts the fuel surface. Fuel corrosion leading to the transition of U^{4+} to U^{6+} will occur from exposure to water vapor regardless of the repository environment; although, the presence of oxygen in the Engineered Barrier System (EBS) environment should lead to higher overall UO_2 oxidation rates (even in the presence of radiolysis). Reducing conditions in the EBS may result in the precipitation of U^{4+}/U^{5+} phases. After 300 years, the β/γ-radiolytic field will be reduced by 3 to 4 orders of magnitude; yet, the dose at the fuel surface from alpha will remain undiminished. Hence, the radiolytic environment adjacent to a relatively fresh (30 yr. old) UNF surface will be little changed from that of an aged (10,000 yr. old) UNF surface exposed to water. This may suggest that experiments on the alteration behavior of UNF today may be relevant for interpreting the possible future condition of UNF in a geologic environment.

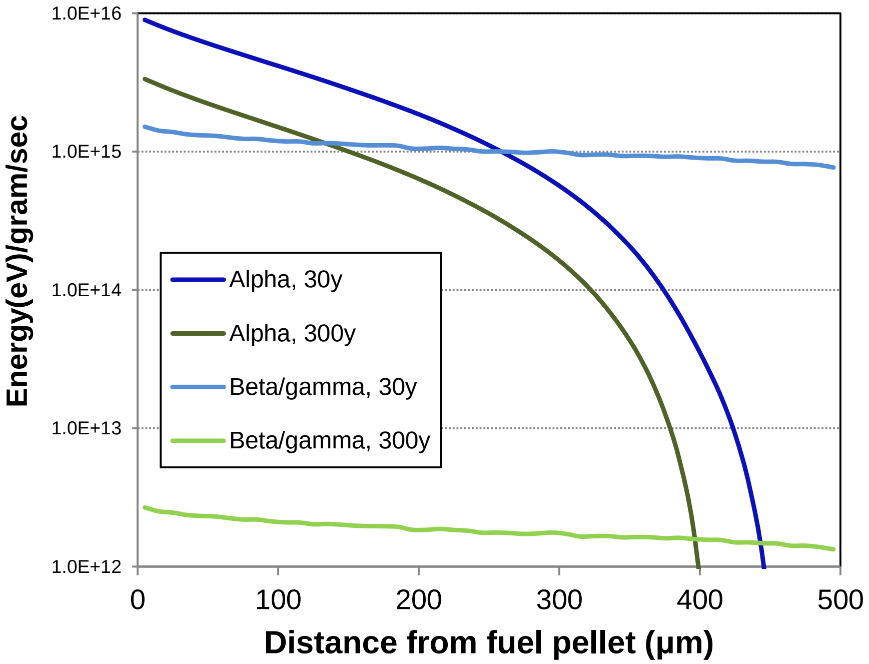

Figure 1.1 The dose to the surface of UNF exposed to a mixed water-air environment (10% water) is dominated by long-lived alpha radiation even at relatively short times out of reactor [Adapted from Radulescu 2011].

1.1 Modeling Concepts and Processes

A model is being developed that can be used to predict the corrosion rate of UO_2 and model the uranyl-carbonate radiolytic system. Initial efforts concentrated on repeating the work of Sunder (1998), Christensen and Sunder (2000), Sunder et al. (1997), and Poinssot et al. (2005) and creating a more inclusive model. We have incorporated the best concepts from the literature to develop a more comprehensive super-set of reactions, and conducted analyses to determine the most important processes under a larger variety of conditions than has been done previously.

A schematic diagram showing the various processes involved in the interaction of ionizing radiation in water is shown in Figure 1.2. In this study, we are concerned mainly with the effectively long time processes that result in the formation of the six radiolytic species. G-values[a] for these species have been established for all forms of ionizing radiation (See Figure 1.2). There is a significant difference in the G value for H_2O_2 in water compared to brine environments and a significant difference in G values between alpha and gamma radiations. Experiments by Cera et al. (2007) have led to the establishment of effective G-values for H_2O_2 generation that consider the effect of iron and UO_2 surfaces; however, such approaches may be inappropriate under different disposal scenarios. King et al. (1999) have developed a mixed potential model for predicting the effects of α-radiolysis, the precipitation of uranyl secondary minerals (e.g., uranophane, schoepite,), and redox processes with Fe(0) and Fe(II) on the dissolution of UO_2. However, these models do not model the formation of oxidants directly but rather assume constant values.

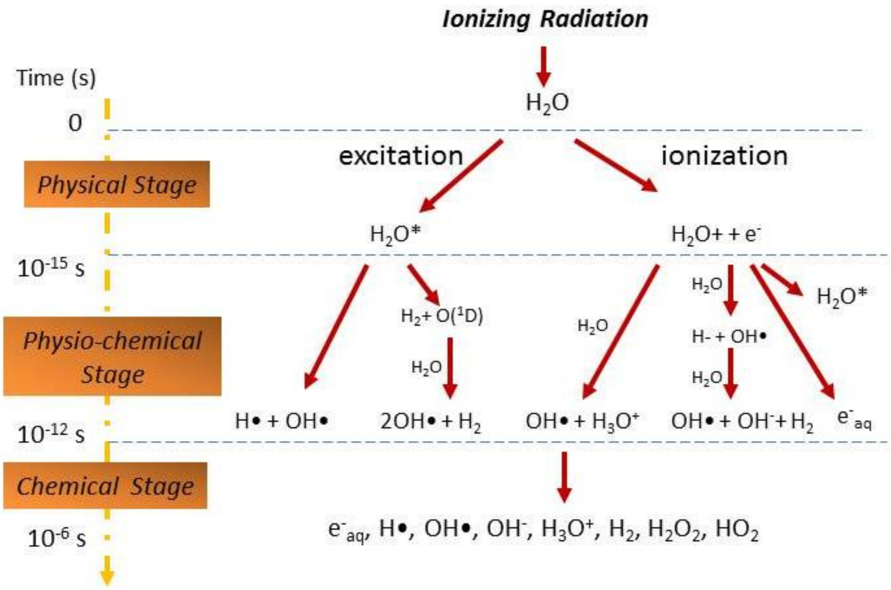
Ionizing Radiation
Time (s)
0
H_2O
excitation
ionization
Physical Stage
H_2O^*
$H_2O^+ + e^-$
10^{-15} s
H_2O
H_2O^*
$H_2 + O(^1D)$
H_2O
$H^- + OH\bullet$
Physio-chemical Stage
H_2O
H_2O
$H\bullet + OH\bullet$
$2OH\bullet + H_2$
$OH\bullet + H_3O^+$
$OH\bullet + OH^- + H_2$
e^-_{aq}
10^{-12} s
Chemical Stage
e^-_{aq}, $H\bullet$, $OH\bullet$, OH^-, H_3O^+, H_2, H_2O_2, HO_2
10^{-6} s

Figure 1.2 Schematic of reaction pathways in the radiolysis model (adapted from Sunder 1998)

Indeed, only H_2O_2 generation was considered in the model in the 1999 version of the mixed potential model developed by King et al. (1999) and Sunder (1998); hence, this model could be improved with a more comprehensive radiolysis component. Most radiolysis modeling has concentrated on gamma irradiation rather than alpha irradiation, and there are few, if any, examples in the literature of radiolytic species predictions under alpha radiolysis.

---

[a] G-value is the number of molecules produced from the deposition of 100 eV into a solution.

As a base model, we considered the reaction kinetics of Christensen and Sunder (2000) applied to the heterogeneous system of UO_2 dissolution at a solid-aqueous boundary. As expected, radiolysis products, increasing with dose rate, have a strong effect on the predicted oxidative dissolution rate. We find that these predicted rates are sensitive to the specifics of the radiolysis chemistry represented. For instance, even the inclusion of the slow reaction:

$$H\bullet + H_2O \rightarrow H_2 + OH\bullet \tag{1}$$

can change the UO_2 dissolution rate by almost a factor of two. Of course, uncertainty in model parameters and reaction mechanisms results in uncertain predictions. We performed a limited analysis to quantify the sensitivity of dissolution rate to model parameters. This will enable identification of where model uncertainty can be reduced to have greatest benefit to predictability. Additionally, these investigations will help identify experiments that can best reduce the driving model uncertainties. In Figure 1.3, radiolysis predictions are shown for fuel corrosion in an anoxic environment and within a thin layer of water. The plot is divided into a time-dependent portion, and the second half shows the concentration of species varying with distance once the system has achieved steady-state conditions. The carbonate level was set at 0.1 mM. H_2O_2 and H_2 concentrations build rapidly and reach steady-state levels at ~15 minutes. These concentrations persist 1 mm from the surface of the fuel; in contrast, the radicals have very short diffusion lengths (see Table 1.2). There is evidence of the formation of persistent oxalate species at extremely low concentrations.

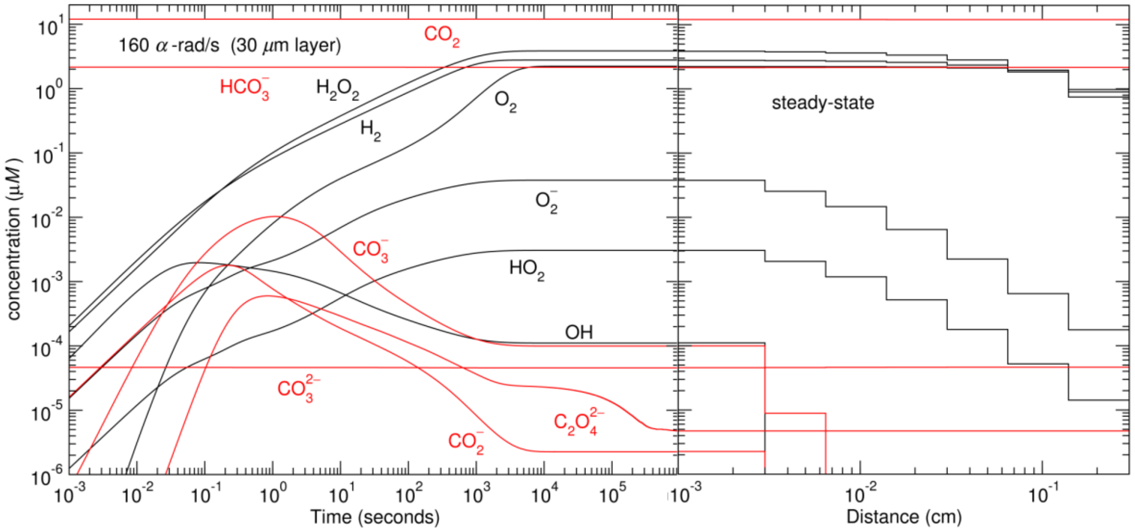

Figure 1.3 Calculated surface environment within 30 mm of a 160 rad/s alpha field in an anoxic environment illustrating the time dependence of dominant species

The early versions of the Pacific Northwest National Laboratory (PNNL) model were verified by using the reactions reported by Pastina and LaVerne (2001) and those of Poinssot et al. (2005) to reproduce their results, which had been done using FACSIMILE[b] and MAKSIMA-CHEMIST[c] kinetic software products. Using the complete list of equations (see Table 1.3 and Table 1.4 for the list of reactions), the match to the Pastina and LaVerne (2001) simulation was unsatisfactory; however, when reaction (1) was removed (see above), the agreement was good. This one reaction results in a large change in the radiolytic species predicted. Without validation by experiment, it is difficult to determine which processes need to be considered. Experimental work on radiolysis will be reported elsewhere. The computational work will help identify future experiments that can best reduce the driving model uncertainties. The model is highly adaptable to other scenarios, including different temperatures, dose, physical environments, gas composition, etc., as long as the appropriate rate equations are available.

The existing radiolytic model has been expanded to include heterogeneous environments consisting of solid-water-layer gas phase and chloride-dominated environments that would be relevant to a generic salt repository. The chloride results have not been included in this model report.

Trummer and Jonnson (2010) have shown that the computational radiolysis simulations indicate that H_2 affects the H_2O_2 concentration during α-radiolysis. The magnitude of the effect depends on the dose rate and the H_2 pressure, as well as on the concentration of HCO_3^-. The following reactions reduce the H_2O_2 concentration in the presence of H_2.

$$\bullet OH + H_2 \rightarrow H_2O + \bullet H \qquad (2)$$

$$\bullet H + H_2O_2 \rightarrow H_2O + \bullet OH \qquad (3)$$

The impact of the radiolytic H_2 effect on the rate of α-radiation induced dissolution of used fuel is discussed along with other (α- and γ-) radiation induced processes capable of reducing the concentration of uranium in solution. Because most anticipated EBS environments will contain bicarbonate (HCO_3^-) in mM concentrations, the radiolytically produced hydroxyl radical will be scavenged according to reaction:

$$\bullet OH + HCO_3^- \rightarrow H_2O + \bullet CO_3^- \qquad (4)$$

---

[b] Developed by Richard Ball and Alan Barton, MCPA software Ltd, United Kingdom.

[c] Developed by Atomic Energy of Canada Ltd., Chalk River (Ontario).

In the presence of H_2, this reaction and reactions (2 and 3) will compete, and hence, the inhibiting effect of H_2 is expected to decrease with increasing HCO_3^-concentration. Ekeroth et al. (2006) have shown that the presence of H_2 (40 bar) in the absence of HCO_3^- reduced the total rate of UO_2 oxidation by a factor of 200. In contrast, in the presence of H_2 and HCO_3^-, however, the total rate of UO_2 oxidation reduced by a factor of 3.5.

Along with ionization, the interaction of energetic radiation with water molecules can generate very short-lived (10^{-15} s) electronic excitations that favorably de-excite through intermediate atomic and molecular radicals. The reaction of these radicals with the surrounding aqueous environment occurs on the scale of 10^{-9} s resulting in several dominant species – both stable and unstable. We take the conventional approach in representing the radiolytic generated species at the later time scale with effective *G*-values. The *G*-values account for the effective fraction of radiative energy that contributes to the formation energy of the dominate radiolytic species. Values for alpha radiolysis used in this work are given in Table 1.1. The concentration of the radiolytic products depends on the dose and on their respective *G*-values. These are source terms to the kinetics equations for each for the species and are represented in Figure 1.2.

Table 1.1 Gamma and alpha particle *G*-values [adapted from Poinssot et al. 2005]

	Gamma		Alpha		5 MeV Alpha[d]
Species	Water	5 M NaCl	Water	5 M NaCl	Water
H_2O_2	0.70	0.09	0.98	0.23	1.00
$\bullet HO_2$	0	0	0.22	0.05	0.10
H_2	0.45	0.60	1.30	1.52	1.20
•H	0.55	0.03	0.21	0.26	0.10
e_{aq}	2.65	3.89	0.06	0.06	0.15
•OH	2.70	0.09	0.25	0.06	0.35
OH^-	0	0	0	1.01	0
H^+	2.65	0.44	0.06	0	0.18
Cl^-	0	-6.26	0	-1.62	0
Cl_2	0	2.43	0	0	0
$ClOH^-$	0	0.38	0	0.55	0
•HClO	0	1.02	0	1.07	0
H_2O	-4.10	-1.67	-2.65	-3.25	–2.58

---

[d] Values used in this model report.

While for shorter fuel decay times the gamma dose is considerably higher for the far-field region around the fuel, the near-field dose at the fuel surface is strongly dominated by alpha dose for decay times greater than 30 years, when it is approximately 160 rad/s for 50 GWd/MTU[e] spent fuel. Consistent with alpha decay radiation, the dose rate is assumed to be nonzero only in the nearest 30 µm to the fuel surface (Figure 1.1). Figure 1.4 shows the spatial regions modeled from near the fuel surface to the external solution boundary considered to be at 0.3 cm. Concentrations in each region are coupled through diffusive currents and are expressed in Equations 5 and 6.

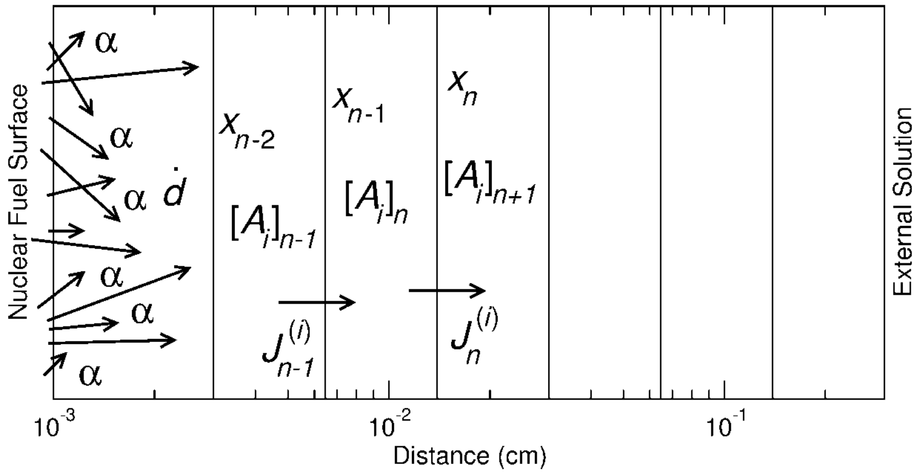

Figure 1.4 Radiolysis Model showing generation and diffusion across spatial regions

The coupled kinetics rate equations for the component concentrations $[A_i]_n$ are

$$\frac{d\,[A_i]_n}{dt} + \frac{J_n^{(i)} - J_{n-1}^{(i)}}{x_n - x_{n-1}} = G_i \dot{d}_n + \sum_{r=1}^{N_r} k_{ir} \prod_{j_r=1}^{n_r} [A_{j_r}]_n^{O_{j_r}} \tag{5}$$

with rate constants k_{ir}, dose rate $\dot{d}_n$ and radiolytic generation constants G_i, where the diffusive currents ($J^{(i)}$) and diffusion constants (D_i) appear in the discretized Fick's Law according to

$$J_n^{(i)} = -2D_i \frac{[A_i]_{n+1} - [A_i]_n}{x_{n+1} - x_{n-1}} \tag{6}$$

for each component *i* in region *n*. Table 1.2 shows the values of diffusion constants used in the model. Table 1.3 and Table 1.4 list the base values for all the reaction rate constants where the numbers in parentheses indicate the negative $\log_{10}$ of the equilibrium constant used with appropriate rate constants to define the reverse reaction rate.

---

[e] GWd/MTU = giga-Watt days per metric tonner of uranium.

Table 1.2 Diffusion constants [Christensen and Sunder 1996] D_i

Species	e^-	$\cdot OH$	O_2^-	H_2O_2	O_2	H_2	Others
D_i ($10^{-5} cm^2 s^{-1}$)	4.9	2.3	1.5	1.9	2.5	6.0	1.5
Sensitivity ($\Delta[H_2O_2]/[H_2O_2]$)	$1 x 10^{-7}$	$5 x 10^{-5}$	0.0052	–25.5	$–1 x 10^{-3}$	–0.275	----

Table 1.3 Water reaction rate constants [Poinssot et al. 2005] ($M^n s^{-1}$)

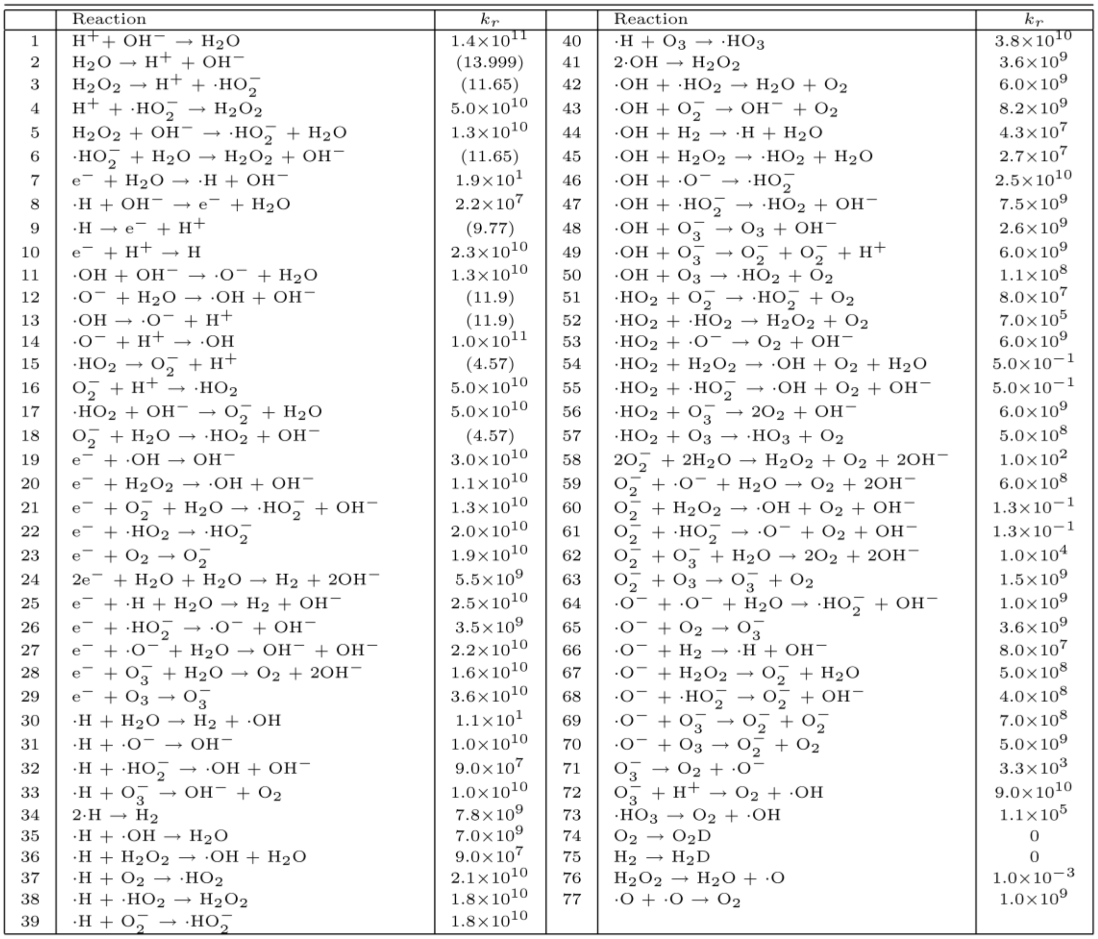

	Reaction	k_r		Reaction	k_r
1	$H^+ + OH^- \rightarrow H_2O$	1.4×10^{11}	40	$\cdot H + O_3 \rightarrow \cdot HO_3$	3.8×10^{10}
2	$H_2O \rightarrow H^+ + OH^-$	(13.999)	41	$2\cdot OH \rightarrow H_2O_2$	3.6×10^{9}
3	$H_2O_2 \rightarrow H^+ + \cdot HO_2^-$	(11.65)	42	$\cdot OH + \cdot HO_2 \rightarrow H_2O + O_2$	6.0×10^{9}
4	$H^+ + \cdot HO_2^- \rightarrow H_2O_2$	5.0×10^{10}	43	$\cdot OH + O_2^- \rightarrow OH^- + O_2$	8.2×10^{9}
5	$H_2O_2 + OH^- \rightarrow \cdot HO_2^- + H_2O$	1.3×10^{10}	44	$\cdot OH + H_2 \rightarrow \cdot H + H_2O$	4.3×10^{7}
6	$\cdot HO_2^- + H_2O \rightarrow H_2O_2 + OH^-$	(11.65)	45	$\cdot OH + H_2O_2 \rightarrow \cdot HO_2 + H_2O$	2.7×10^{7}
7	$e^- + H_2O \rightarrow \cdot H + OH^-$	1.9×10^{1}	46	$\cdot OH + \cdot O^- \rightarrow \cdot HO_2^-$	2.5×10^{10}
8	$\cdot H + OH^- \rightarrow e^- + H_2O$	2.2×10^{7}	47	$\cdot OH + \cdot HO_2^- \rightarrow \cdot HO_2 + OH^-$	7.5×10^{9}
9	$\cdot H \rightarrow e^- + H^+$	(9.77)	48	$\cdot OH + O_3^- \rightarrow O_3 + OH^-$	2.6×10^{9}
10	$e^- + H^+ \rightarrow H$	2.3×10^{10}	49	$\cdot OH + O_3^- \rightarrow O_2^- + O_2^- + H^+$	6.0×10^{9}
11	$\cdot OH + OH^- \rightarrow \cdot O^- + H_2O$	1.3×10^{10}	50	$\cdot OH + O_3 \rightarrow \cdot HO_2 + O_2$	1.1×10^{8}
12	$\cdot O^- + H_2O \rightarrow \cdot OH + OH^-$	(11.9)	51	$\cdot HO_2 + O_2^- \rightarrow \cdot HO_2^- + O_2$	8.0×10^{7}
13	$\cdot OH \rightarrow \cdot O^- + H^+$	(11.9)	52	$\cdot HO_2 + \cdot HO_2 \rightarrow H_2O_2 + O_2$	7.0×10^{5}
14	$\cdot O^- + H^+ \rightarrow \cdot OH$	1.0×10^{11}	53	$\cdot HO_2 + \cdot O^- \rightarrow O_2 + OH^-$	6.0×10^{9}
15	$\cdot HO_2 \rightarrow O_2^- + H^+$	(4.57)	54	$\cdot HO_2 + H_2O_2 \rightarrow \cdot OH + O_2 + H_2O$	5.0×10^{-1}
16	$O_2^- + H^+ \rightarrow \cdot HO_2$	5.0×10^{10}	55	$\cdot HO_2 + \cdot HO_2^- \rightarrow \cdot OH + O_2 + OH^-$	5.0×10^{-1}
17	$\cdot HO_2 + OH^- \rightarrow O_2^- + H_2O$	5.0×10^{10}	56	$\cdot HO_2 + O_3^- \rightarrow 2O_2 + OH^-$	6.0×10^{9}
18	$O_2^- + H_2O \rightarrow \cdot HO_2 + OH^-$	(4.57)	57	$\cdot HO_2 + O_3 \rightarrow \cdot HO_3 + O_2$	5.0×10^{8}
19	$e^- + \cdot OH \rightarrow OH^-$	3.0×10^{10}	58	$2O_2^- + 2H_2O \rightarrow H_2O_2 + O_2 + 2OH^-$	1.0×10^{2}
20	$e^- + H_2O_2 \rightarrow \cdot OH + OH^-$	1.1×10^{10}	59	$O_2^- + \cdot O^- + H_2O \rightarrow O_2 + 2OH^-$	6.0×10^{8}
21	$e^- + O_2^- + H_2O \rightarrow \cdot HO_2^- + OH^-$	1.3×10^{10}	60	$O_2^- + H_2O_2 \rightarrow \cdot OH + O_2 + OH^-$	1.3×10^{-1}
22	$e^- + \cdot HO_2 \rightarrow \cdot HO_2^-$	2.0×10^{10}	61	$O_2^- + \cdot HO_2^- \rightarrow \cdot O^- + O_2 + OH^-$	1.3×10^{-1}
23	$e^- + O_2 \rightarrow O_2^-$	1.9×10^{10}	62	$O_2^- + O_3^- + H_2O \rightarrow 2O_2 + 2OH^-$	1.0×10^{4}
24	$2e^- + H_2O + H_2O \rightarrow H_2 + 2OH^-$	5.5×10^{9}	63	$O_2^- + O_3 \rightarrow O_3^- + O_2$	1.5×10^{9}
25	$e^- + \cdot H + H_2O \rightarrow H_2 + OH^-$	2.5×10^{10}	64	$\cdot O^- + \cdot O^- + H_2O \rightarrow \cdot HO_2^- + OH^-$	1.0×10^{9}
26	$e^- + \cdot HO_2^- \rightarrow \cdot O^- + OH^-$	3.5×10^{9}	65	$\cdot O^- + O_2 \rightarrow O_3^-$	3.6×10^{9}
27	$e^- + \cdot O^- + H_2O \rightarrow OH^- + OH^-$	2.2×10^{10}	66	$\cdot O^- + H_2 \rightarrow \cdot H + OH^-$	8.0×10^{7}
28	$e^- + O_3^- + H_2O \rightarrow O_2 + 2OH^-$	1.6×10^{10}	67	$\cdot O^- + H_2O_2 \rightarrow O_2^- + H_2O$	5.0×10^{8}
29	$e^- + O_3 \rightarrow O_3^-$	3.6×10^{10}	68	$\cdot O^- + \cdot HO_2^- \rightarrow O_2^- + OH^-$	4.0×10^{8}
30	$\cdot H + H_2O \rightarrow H_2 + \cdot OH$	1.1×10^{1}	69	$\cdot O^- + O_3^- \rightarrow O_2^- + O_2^-$	7.0×10^{8}
31	$\cdot H + \cdot O^- \rightarrow OH^-$	1.0×10^{10}	70	$\cdot O^- + O_3 \rightarrow O_2^- + O_2$	5.0×10^{9}
32	$\cdot H + \cdot HO_2^- \rightarrow \cdot OH + OH^-$	9.0×10^{7}	71	$O_3^- \rightarrow O_2 + \cdot O^-$	3.3×10^{3}
33	$\cdot H + O_3^- \rightarrow OH^- + O_2$	1.0×10^{10}	72	$O_3^- + H^+ \rightarrow O_2 + \cdot OH$	9.0×10^{10}
34	$2\cdot H \rightarrow H_2$	7.8×10^{9}	73	$\cdot HO_3 \rightarrow O_2 + \cdot OH$	1.1×10^{5}
35	$\cdot H + \cdot OH \rightarrow H_2O$	7.0×10^{9}	74	$O_2 \rightarrow O_2D$	0
36	$\cdot H + H_2O_2 \rightarrow \cdot OH + H_2O$	9.0×10^{7}	75	$H_2 \rightarrow H_2D$	0
37	$\cdot H + O_2 \rightarrow \cdot HO_2$	2.1×10^{10}	76	$H_2O_2 \rightarrow H_2O + \cdot O$	1.0×10^{-3}
38	$\cdot H + \cdot HO_2 \rightarrow H_2O_2$	1.8×10^{10}	77	$\cdot O + \cdot O \rightarrow O_2$	1.0×10^{9}
39	$\cdot H + O_2^- \rightarrow \cdot HO_2^-$	1.8×10^{10}			

Some reactions such as 74 and 75[f] are present to make comparisons with results from other studies and are intentionally set to zero here for physical consistency. Figure 1.3 shows the time dependence (left side) and steady-state spatial dependence (right side) of the highest concentration species for a surface alpha dose of 160 rad/s. In this case the initial O_2 concentration was assumed to be zero to represent an oxygen-depleted environment that might reflect repository conditions that are externally reducing.

Table 1.4 Carbonate reaction rate constants [Poinssot et al. 2005] ($M^n s^{-1}$)

	Reaction	k_r		Reaction	k_r
78	$H^+ + CO_3^{2-} \rightarrow HCO_3^-$	5.0×10^{10}	96	$CO_2^- + H_2O_2 \rightarrow CO_2 + OH^- + \cdot OH$	7.3×10^5
79	$CO_2 + H_2O \rightarrow H^+ + HCO_3^-$	7.0×10^1	97	$CO_2^- + HCO_3^- \rightarrow HCO_2^- + \cdot CO_3^-$	1.0×10^3
80	$H^+ + HCO_3^- \rightarrow CO_2 + H_2O$	1.0×10^{10}	98	$C_2O_6^{2-} \rightarrow C_2O_4^{2-} + O_2$	1.0×10^0
81	$HCO_3^- \rightarrow CO_3^{2-} + H^+$	2.0×10^0	99	$C_2O_6^{2-} \rightarrow \cdot HO_2^- + OH^- + 2CO_2 - H_2O$	2.0×10^2
82	$CO_2 + e^- \rightarrow CO_2^-$	7.7×10^9	100	$\cdot CO_3^- + C_2O_4^{2-} \rightarrow C_2O_4^- + CO_3^{2-}$	3.0×10^3
83	$HCO_3^- + \cdot OH \rightarrow \cdot CO_3^- + H_2O$	8.5×10^6	101	$C_2O_4^{2-} + e^- \rightarrow C_2O_4^{3-}$	0
84	$CO_3^{2-} + \cdot OH \rightarrow \cdot CO_3^- + OH^-$	3.9×10^8	102	$C_2O_4^{2-} + \cdot OH \rightarrow C_2O_4^- + OH^-$	7.7×10^6
85	$HCO_3^- + \cdot H \rightarrow H_2 + \cdot CO_3^-$	4.4×10^4	103	$C_2O_4^- + C_2O_4^- \rightarrow 2CO_2 + C_2O_4^{2-}$	4.8×10^8
86	$CO_3^{2-} + e^- \rightarrow CO_2^- + 2OH^- - H_2O$	3.9×10^5	104	$C_2O_4^- + O_2 \rightarrow O_2^- + CO_2 + CO_2$	$5.\times10^9$
87	$\cdot CO_3^- + \cdot CO_3^- \rightarrow C_2O_6^{2-}$	1.4×10^7	105	$C_2O_4^- \rightarrow CO_2 + CO_2^-$	0
88	$\cdot CO_3^- + \cdot CO_3^- \rightarrow CO_2 + CO_4^{2-}$	$7.\times10^6$	106	$\cdot CO_3^- + HCO_2^- \rightarrow HCO_3^- + CO_2^-$	1.5×10^5
89	$\cdot CO_3^- + H_2O_2 \rightarrow CO_3^{2-} + O_2^- + 2H^+$	9.8×10^5	107	$HCO_2^- + \cdot OH \rightarrow H_2O + CO_2^-$	3.2×10^9
90	$\cdot CO_3^- + \cdot HO_2^- \rightarrow CO_3^{2-} + O_2^- + H^+$	1.0×10^7	108	$HCO_2^- + \cdot H \rightarrow H_2 + CO_2^-$	2.1×10^8
91	$\cdot CO_3^- + O_2^- \rightarrow CO_3^{2-} + O_2$	4.0×10^8	109	$HCO_2^- + e^- \rightarrow H_2 + CO_2^- - H^+$	8.0×10^8
92	$\cdot CO_3^- + CO_2^- \rightarrow CO_3^{2-} + CO_2$	3.0×10^8	110	$OH^- + HCO_3^- \rightarrow CO_3^{2-} + H_2O$	1.0×10^9
93	$CO_2^- + e^- \rightarrow HCO_2^- + OH^- - H_2O$	1.0×10^9	111	$CO_3^{2-} + H_2O \rightarrow OH^- + HCO_3^-$	3.6×10^3
94	$CO_2^- + CO_2^- \rightarrow C_2O_4^{2-}$	6.5×10^8	112	$\cdot CO_3^- + \cdot CO_3^- \rightarrow CO_4^{2-} + CO_2$	7.0×10^6
95	$CO_2^- + O_2 \rightarrow CO_2 + O_2^-$	2.0×10^9	113	$H_2O + CO_4^{2-} \rightarrow \cdot HO_2^- + CO_2 + OH^-$	2.0×10^{-1}

The concentrations of unstable species are seen to decrease in regions away from the fuel surface where they are generated (right side of Figure 1.3). The bottom row of Table 1.2 shows that the concentration of H_2O_2 would be about 25 times greater without diffusion.

---

[f] The 'D' in equations 74 and 75 represents the loss of O_2 and H_2 from the system through diffusion (see Christensen and Sunder 2000).

2. Verification, Validation, and Sensitivity Analyses

Radiolytic models do not have a wide acceptance for heterogeneous systems due to limited availability of kinetic data, the difficulty in handling interfaces, and a lack of experimental validation. It is important to note that there were no examples in the literature of radiolytic modeling simulations with alpha irradiation that would have provided a basis for comparison; hence, the current PNNL model was verified against other radiolysis models by using gamma irradiation simulations. To build confidence in the use of the PNNL computational radiolysis model, it was also necessary to compare consistency between existing kinetic models. Poinssot et al. (2005) compared the results from “CHEMSIMUL” and “MAKSIMA-CHEMIST”. In the worst case, the differences were < 1%, and these were because of the different integration methods used for resolving the differential equations, numerical precision used in each code, the number of significant figures used in the G-values and kinetics constants. Figure 2.1 shows an examples from Pastina and LaVerne (2001, Figure 1) where it was possible to duplicate their result with the PNNL program.

During development the radiolysis model has been tested for its internal consistency and for predictions that are verifiable with available models in the literature (Christian and Sunder 2000, Erschov and Gordeev 2008). The PNNL model is organized for internal checking of atom and charge balance. Both total atoms and charge were shown to balance within relative solution accuracy of ~10^{-10}. The basic model solver is a routine from ODEPACK (Hindmarsh 1983, Petzold 1983) for solving stiff and non-stiff ordinary differential equations. Solution run-times for concentration histories out to 10^8 seconds normally run in under 1 minute on a single processor desktop computer.

The methodology of coding the reaction equations was verified by comparing model results to published results of other models for specific cases. Three cases are reported here and in all instances, the ionizing radiation was gamma because there are no literature model predictions using alpha irradiation.

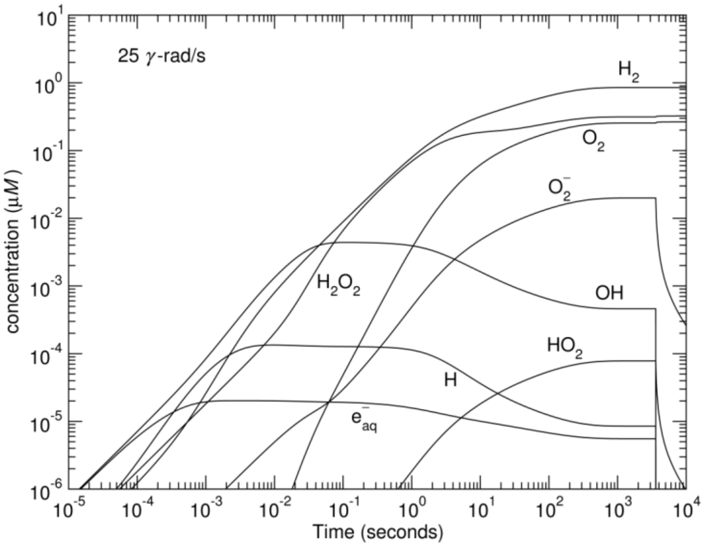

Figure 2.1 Concentration history results for the same conditions (1 hr., 25 rad/s irradiation) as Pastina and LaVerne (2001, Figure 1).

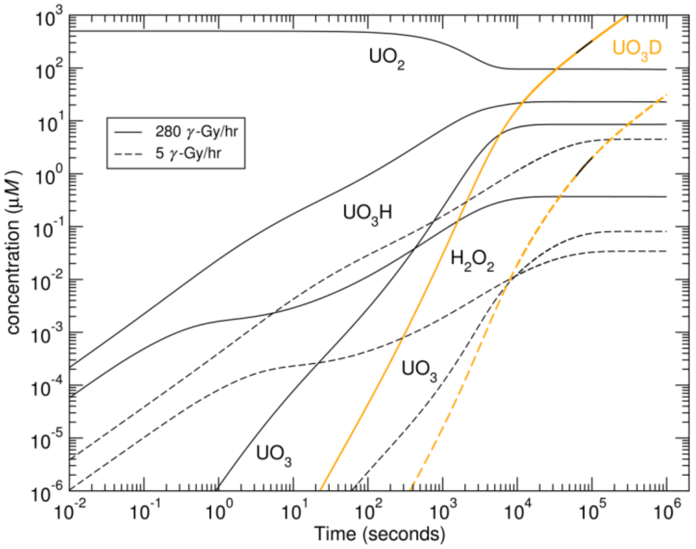

Figure 2.2 Radiolysis model result with inputs from Christensen and Sunder (2000)

Figure 2.2 shows the concentration history results as a function of time for the conditions reported in Christensen and Sunder (2000, Figure 9a and 9b). The UO_2 dissolution rates reported by Christensen and Sunder (2000) were shown to be the same as those from the PNNL model using the same input parameters verifying consistency between the computational approaches.

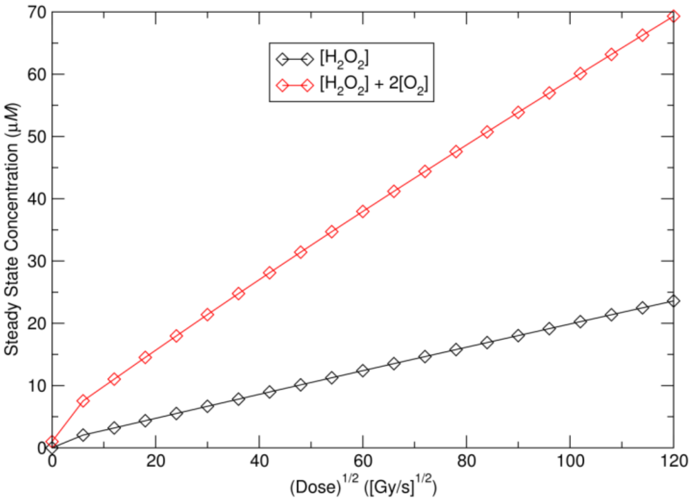

Figure 2.3 Radiolysis model result for gamma irradiation with inputs from Ershov and Gordeev (2008)

Figure 2.3 shows the model results for the steady-state concentration as a function of the square-root of dose for the conditions reported by Ershov and Gordeev (2008, Figure 5). In each of the three cases the model results reported here are nearly indistinguishable from the results reported in the figures of each of the three references. Note that there is a predicted square root dose dependence for H_2O_2 under gamma irradiation; whereas, we have shown that there is a linear dependence with dose under alpha irradiation. However, there are currently no alpha irradiation studies upon which to validate the PNNL model approach.

3. Uncertainty and Conditional Applicability

Identification of the most sensitive parameters for steady-state H_2O_2 concentration were determined as the relative change $\Delta[H_2O_2]/[H_2O_2]$ for each parameter – the relative difference between model results with non-zero and zero value for a parameter. As already mentioned, the bottom row of Table 1.2 shows the sensitivity of $[H_2O_2]$ to the diffusion constants. Figure 3.1 is the sensitivity result of three oxidizing species for each *G*-value. Of course $[H_2O_2]$ is most sensitive to its own *G*-value – the O_2 concentration is also sensitive to the H_2O_2 *G*-value because H_2O_2 decomposition is a source for O_2. Also, because the •OH radical and OH^- ion can react with H_2O_2, their *G*-values result in a negative change for $[H_2O_2]$. This is consistent with the small positive change for the •OH diffusion constant (Table 1.2), i.e. H_2O_2 is increased slightly because •OH diffuses away from the production region.

To evaluate the relative importance of all equations shown in Table 1.3 on the steady-state concentration of H_2O_2, each reaction was switched off independently and allowed to run until steady-state conditions were reached. The resulting plot is shown in Figure 3.2 and shows the absolute value of the relative change in $[H_2O_2]$ with the top reactions (i.e., above the red line) shown as red/black for +/– values. Removal of all reactions below the horizontal red line, which represents relative changes of less than 1 in 10^5 for the H_2O_2, results in no perceptible changes to concentrations in Figure 1.4 other than oxalate $[(C_2O_4)^{2-}]$.

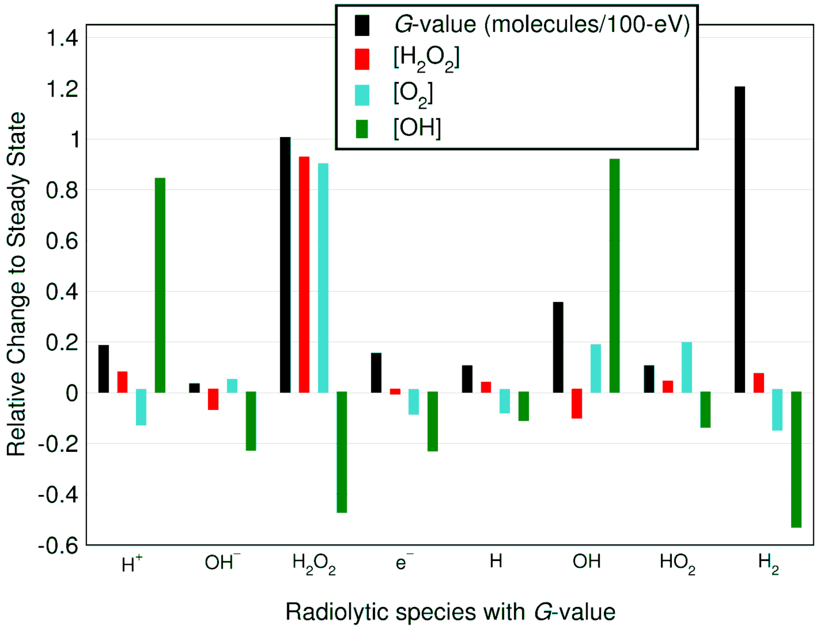

Figure 3.1 *G*-value sensitivity as $\Delta[A]/[A]$ for H_2O_2, H_2O_2 & •OH

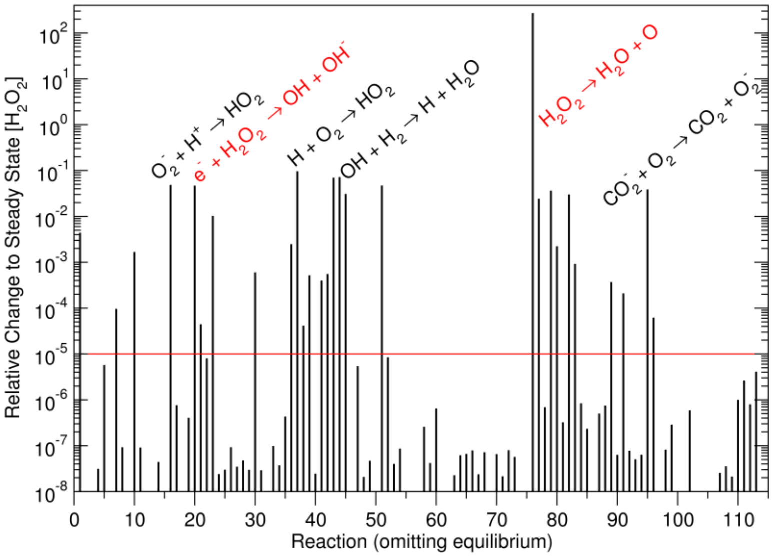

Figure 3.2 Rate constant sensitivity as absolute value of $\Delta[H_2O_2]/[H_2O_2]$

An important result for input into other corrosion models is the total concentration of H_2O_2 with dose. In Figure 3.3, the linear relationship between dose and the steady-state H_2O_2 oxidant concentration is shown. This relationship holds for a range of H_2 concentrations. There was only a slight difference beginning to show between the full and reduced parameter set at very high doses.

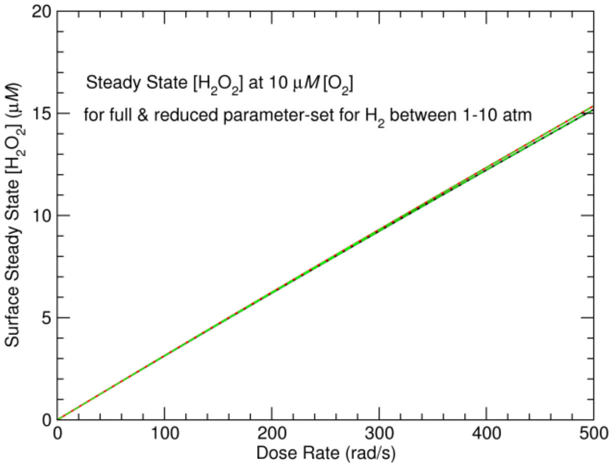

Figure 3.3 H_2O_2 concentration as a function of dose for fixed O_2 concentration and range of H_2 concentrations

During investigation of the steady-state concentration of H_2O_2 under anoxic conditions with changing radiation dose, it was observed that there was a sudden change in the H_2O_2 concentration at a critical dose value. The actual position of this jump varied depending on the initial conditions. The specific initial conditions require zero O_2 concentration. Figure 3.4 (right) is a case with H_2 concentration fixed at 7.8×10^{-4} *M* (0.1 atm) were the jump occur between 141 and 142 rad/s. It was determined that at least two steady-state solutions to the kinetic equations exist for dose rates greater than 142 rad/s. This can be seen in Figure 3.4 (left side), where the dashed (pink) and solid (pink) lines are steady-state solutions for the same conditions (water system 0.1 atm H_2) with the only difference being a non-zero oxygen concentration for the dashed line result. This is an example where the model loses its ability to uniquely predict the $[H_2O_2]$; hence, we consider the condition of exactly zero $[O_2]$ to be outside the applicability of the current PNNL model.

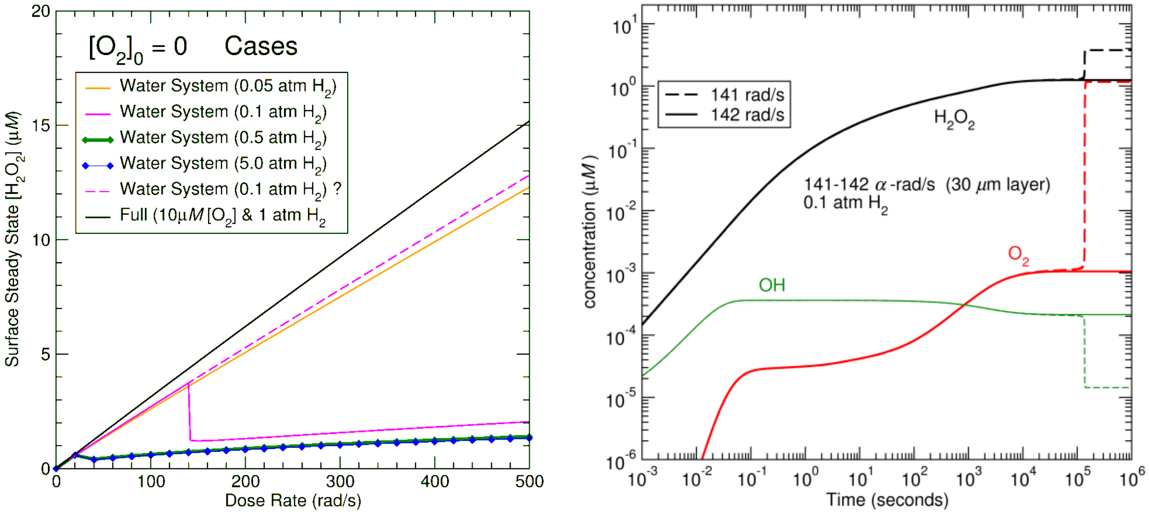

Figure 3.4 H_2O_2 concentration as a function of dose rate for cases of *zero* initial O_2 concentration

Both the full and reduced set of reactions exhibited these non-unique steady-state solutions at critical values of dose rate for initially very low concentrations of $[O_2]$ and $[H_2]$. The reasons for this effect need to be examined in greater depth and should be validated through experiment.

3.1 Hydrogen

An important environmental constraint in the used fuel dissolution model is the potential stabilizing effect of H_2, mainly from canister corrosion and, to a lesser extent, from radiolysis. Consideration of H_2 formation in the water just from radiolysis may not to be sufficient to describe the experimentally observed H_2 effect (Carbol et al. 2009). Experiments by Pastina and LaVerne (2001) that examined the generation of H_2 and H_2O_2 under irradiation indicated that there remain significant uncertainties regarding the basic reactions. The potential catalytic role of metallic epsilon particles was considered by the model by Erschov and Gordeev (2008) resulting in faster consumption of H_2. The European models (Poinssot et al. 2005) all show a strong reduction of reaction rates with increasing H_2 concentration. The reasons for this rate reduction in relation to H_2 pressure is an active area of research. The current model predicts the achievement of a steady-state U concentration at high H_2 pressures. For long-term predictions, significant differences are expected when comparing long-term solubility or rate control. In addition to radiolysis, hydrogen can be generated by anoxic corrosion of various metal components of the waste and packaging (primarily iron-based materials) (Carbol et al. 2009). Anoxic conditions can only be expected under inundated conditions, where brine has somehow accumulated and completely surrounds the waste. Estimates of the rates of hydrogen production under anoxic and fully brine-inundated conditions may be made; however, these rates are quite uncertain. After initial closure of a panel, oxygen-rich conditions will prevail, and the iron will oxidize (rust) with no hydrogen generation possible until all of the oxygen has been consumed. The oxidation rate is highly dependent on humidity as well. The low humidity in a potential salt repository will minimize oxidation. The accumulation of hydrogen is mitigated by its ease of diffusion through even highly impermeable materials.

3.2 The Role of Bicarbonate and Oxalate Formation

Carbonate is known to strongly enhance dissolution of oxidized spent fuel. The radiolysis model included the effect of HCO_3 on the radiolytic reaction scheme. The heterogeneous model considers fuel oxidation and dissolution separately; whereas, the European models do not include these effects. The observation of oxalate formation at trace levels indicates that the presence of CO_2 could result in the formation of complexing agents that could increase the solubility of some radionuclides.

3.3 Secondary Uranium phases

The deposition of secondary phases at the UO_2 surface may strongly limit the quantity of water that is accessible at the fuel surface for radiolytic processes. Diffusion of radiolytic species to the non-oxidized fuel is probably strongly limited. The model did not account explicitly for this effect, but it might be possible to include by considering diffusion parallel to the fuel surface and in the presence of lower quantities of water. Experimental data from Carbol et al. (2009) suggests that the corrosion potential is sufficiently low that no formation of U(VI) solid phases will occur. Under these conditions solid-state oxidation products, such as UO_{2+x} and U_3O_7, may still form. However, the reaction of UO_2 to form U_3O_7 is not a dissolution/precipitation process, but better described as a solid-state transformation that would create some kind of boundary layer. This boundary would not impact alpha radiolysis because there would be no significant compositional change during the transformation.

3.4 Brine

The early radiolysis processes in concentrated NaCl brine are different from those in diluted aqueous solutions. Whereas sodium ion (Na^+) under irradiation is chemically inert, the chloride anion (Cl^-) reacts very efficiently with oxidizing radicals. Because of the high Cl- concentration, such reactions will occur in the radiation spurs. With less radical recombination in the spurs- the total yield of species diffusing out of the spurs increases. Furthermore, there is a change in the species spectrum reaching a homogeneous distribution and becoming available for other reactants. In contrast to dilute solutions, there is a direct radiation effect on the solute in concentrated-chloride brine. From the number of electrons attached to the Cl- ions compared to all electrons present in the solvent and the solute, a portion of 15% for the direct effect on Cl- can be estimated for 5 M NaCl solution.

4. Conclusions and Recommendations

- The H_2O_2 G-value has the greatest effect on the steady-state [H_2O_2] (with small negative effect from the •OH radical).
- Only 45 to 46 reactions of the water-carbonate system are important (out of ≈120) for determining [H_2O_2].
- Determining [H_2O_2] to within 0.1% is possible with 22 reactions of the water-carbonate system
- Concentration of H_2 has very small effect on [H_2O_2] as a function of dose rate (with O_2 present) and is linear.
- For extremely low [O_2], nonlinear effects were observed in both water only and water-carbonate systems (even for the reduced parameter set).
- Future investigation will examine merging the PNNL Radiolysis Model with the Mixed Potential Model being developed at Argonne National Laboratory to determine the explicit sensitivity on UO_2 stability in a disposal environment.

Assuming that steady-state H_2O_2 is the dominant oxidant for spent nuclear fuel in an O_2-depleted water environment, the most sensitive parameters have been identified with respect to predictions of a radiolysis model under typical conditions. Compared with the full model with about 100 reactions, it was found that only 30 to 40 of the reactions (above red line of Figure 3.2) are required to determine [H_2O_2] to one part in 10^{-5} and to preserve most of the predictions for major species. This allows a systematic approach for model simplification and offers guidance in designing experiments for validation. For instance, an experiment that accurately measures H_2O_2 decomposition could have a significant effect on improving model accuracy. The approach described here will be applied to the prediction of the fuel behavior of the combined models to assess how the corrosion processes may affect the sensitivities to radiolysis model parameters.

In an anoxic water-dominated geologic repository, H_2O_2 will be the most important oxidizing species that is produced from the radiolysis of water in contact with used nuclear fuel. In a brine system, other oxidants may be more important. Understanding the mechanisms involved in the production of oxidants is important both from a fundamental science perspective and for performance assessment calculations for long-term storage. Recently, Roth and Laverne (2011) have shown larger effects on G(H_2O_2) have been observed in the presence of nanoparticles of various metal oxides, similar to earlier studies on the role of heterogeneous interfaces in radiolytic environments. These types of effects may be more difficult to model and will require experiments to obtain fundamental data for the more advanced repository models.

Although the PNNL radiolysis model is being used to describe potential radiolytic processes that may occur in the unlikely case of groundwater directly contacting a failed nuclear fuel storage package at some distant time in the future, the model is highly adaptable to other scenarios. Under fuel storage conditions, doses will be dominated by gamma fields rather than alpha fields, the temperature will be considerably higher than for a disposal environment, the physical environments will be different, as well as the gas composition. However, as long as the appropriate rate constants are available for the relevant processes, this model could be easily applied to fuel storage environments.

References

Burns, P. C., R. C. Ewing, and A. Navrotsky, 2012. Nuclear fuel in a reactor accident, *Science*, 335: 1184-1188.

Carbol, P., P. Fors, S. Van Winckel, and K. Spahiu. 2009. Corrosion of irradiated MOX fuel in presence of dissolved H_2. *Journal of Nuclear Materials*, 392: 45-54

Cera, E., J. Bruno, and L. Duro, 2007. Experimental determination and chemical modeling of radiolytic processes at the spent fuel /water interface, Svensk Karnbranslehantering AB Report, TR-06-07, Stockholm, Sweden.

Christensen, H., and S. Sunder. 2000. Current state of knowledge of water radiolysis effects on spent nuclear fuel corrosion. *Nuclear Technology* 131: 102-123.

Christensen, H, and S. Sunder. 1996. An evaluation of water layer thickness effective in oxidation of UO_2 fuel due to radiolysis of water, *Journal of Nuclear Materials*, 298: 70-77.

Cui, D., V. V. Rondinella, J. A. Fortner, A. J. Kropf, L. Eriksson, D. J. Wronkiewicz, and K. Spahiu, 2012. Characterization of alloy particles extracted from spent nuclear fuel, *Journal of Nuclear Materials*, 420: 328-333.

Ekeroth, E., O. Roth, and M. Jonsson, 2006. The relative impact of radiolysis products in radiation induced oxidative dissolution of UO_2, *Journal of Nuclear Materials* 355: 38–46

Ershov, B. G., and A.V. Gordeev, 2008. A model for radiolysis of water and aqueous solutions of H_2, H_2O_2 and O_2, *Radiation Physics and Chemistry*, 77: 928-935.

Hughes-Kubatko, K-A., K. B. Helean, A. Navrotsky, and P.C. Burns. 2003. Stability of peroxide-containing uranyl minerals. *Science* 302: 1191-1193.

Jégou , C., B. Muzeau, V. Broudic, S. Peuget,A. Poulesquen, D. Roudil, and C. Corbel. 2005. Effect of external gamma irradiation on dissolution of the spent UO_2 fuel matrix. *Journal of Nuclear Materials* 341: 62–82.

Hindmarsh, A. C., 1983. ODEPACK, A Systematized Collection of ODE Solvers, in Scientific Computing, R. S. Stepleman et al. (Eds.), North-Holland, Amsterdam, pp. 55-64.

King, F., M. Kolar, and D. W. Shoesmith. 1999. Modeling the oxidative dissolution of UO_2. *Materials Research Society Symposium Proceedings* 556: 463-470.

Pastina, B., and J. A. LaVerne, 2001. Effect of molecular hydrogen on hydrogen peroxide in water radiolysis, *Journal of Physics and Chemistry,* B105: 9316-9322.

Petzold, L. R., 1983. Automatic Selection of methods for solving stiff and nonstiff systems of ordinary Differential Equations, *Journal on Scientific and Statistical Computing*, 4: 136-148.

Poinssot, C., C. Ferry, M. Kelm, B. Grambow, A. Martinez, L. Johnson, Z. Andriambolona, J. Bruno, C. Cachior, J. M. Cavedon, H. Christensen, C. Corbel, C. Jegou, K. Lemmens, A. Loida, P. Lovera, F. Miserque, J. de Pablo, A. Poulesquen, J. Quinones, V. Rondinella, K. Spahiu, and D. H. Wegen, 2005. Spent Fuel Stability under Repository Conditions – Final Report of the European Project, European Commission.

Radulescu, G., 2011. Radiation *Transport Evaluations for Repository Science*, ORNL/LTR-2011/294, Oak Ridge National Laboratory, August, 2011.

Roth, O. and Laverne, J. A. 2011. Effect of pH on H_2O_2 production in the radiolysis of water, *Journal of Physics and Chemistry*, A115: 700-708.

Shoesmith, D. W., M. Kolar, and F. King, 2003. A mixed-potential model to predict fuel (uranium dioxide) corrosion within a failed nuclear waste container, *Corrosion,* 59: 802-816.

Stroes-Gascoyne, S., F. Garisto, and J.S. Betteridge. 2005. The effects of alpha-radiolysis on UO_2 dissolution determined from batch experiments with ^{238}Pu-doped $UO_{2.}$ *Journal of Nuclear Materials* 346: 5-15.

Sunder, S., D.W. Shoesmith, and N.H. Miller. 1997. Oxidation and dissolution of nuclear fuel (UO_2) by the products of the alpha radiolysis of water. J*ournal of Nuclear Materials* 244: 66-74.

Sunder, S. 1998. Calculation of radiation dose rates in a water layer in contact with used CANDU UO_2 fuel, *Nuclear Technology* 122: 211-221.

Trummer, M., and M. Jonsson. 2010. Resolving the H_2 effect on radiation induced dissolution of UO_2-based spent nuclear fuel. *Journal of Nuclear Materials* 396: 163–169

ACKNOWLEDGEMENTS

The work summarized in this report was conducted at Pacific Northwest National Laboratory. Programmatic guidance provided by D. Sassani (Sandia National Laboratory) and J. Buelt (PNNL) is also gratefully acknowledged.